Symmetry-enforced band nodes in 230 space groups

Lin Wu, Feng Tang,* and Xiangang Wan

National Laboratory of Solid State Microstructures and School of Physics, Nanjing University, Nanjing 210093, China and Collaborative Innovation Center of Advanced Microstructures, Nanjing University, Nanjing 210093, China

(Received 22 February 2021; accepted 15 June 2021; published 6 July 2021)

Crystallographic symmetries enforcing band touchings (BTs) in the Brillouin zone (BZ) have been utilized to classify and predict the topological semimetals. Though the early proposed topological semimetals contain isolated nodal points in the BZ, the proposed nodal line semimetals later could host various structures of several nodal lines/loops: Nodal chains, nodal nets or Hopf links, etc. In this work, using compatibility relations, we first list all possible high-symmetry lines (HSLs) that can be nodal lines itself, high-symmetry planes (HSPLs) that can host nodal loops, and HSPLs that are nodal surfaces for all 230 space groups (SGs), with spin-orbit coupling and time-reversal symmetry considered or not. We then show how to diagnose a nodal loop from the band crossing in an HSL, or nodal line/surface from irreducible representation (irrep) of a high-symmetry point (HSP), while the rest cases correspond to nodal points. Among our results, those essential cases, for which the nodal points/lines/loops/surfaces must exist, are highlighted since they are promising for the realizations of (nearly) ideal nodal point/line/loop/surface semimetals, as well as systems with flexible tunability owning fixed structure of topological nodal points/lines/loops/surfaces. Based on our results, SGs allowing Hopf-link structure with one straight nodal line threading a nodal loop, or two nesting nodal loops lying in two respective HSPLs, are highlighted, with the predicted materials being $B_5Pb_2IO_9$ in SG 34 and $SrAl_2Au_3$ in SG 62, respectively. Our exhaustive results could serve as a useful guide for efficiently predicting and designing materials or artificial systems owning exotic geometric nodal structures of energy bands simply based on structure symmetries.

DOI: 10.1103/PhysRevB.104.045107

I. INTRODUCTION

Over the past fifteen years, topological materials in condensed physics have attracted broad interest due to their novel properties related with the nontrivial band topology and potential in device applications with low-energy consumptions [1–6]. Symmetry, e.g., time-reversal symmetry (TRS) and space group (SG) symmetry, plays a vital role in the classification, protection or prediction of various topological phases in realistic materials [7–12]. As with TRS that protects $\mathbb{Z}_2$ strong topological insulators, crystallographic symmetry could protect topological crystalline insulators (TCIs) with fancy degeneracies on symmetry-respected boundaries [13,14]. The fruitful crystallographic symmetries in 230 SGs for three dimensional (3D) systems thus give rise to various TCIs: mirror Chern insulators [15], hourglass insulators [16], higher-order topological insulators [17–20], TCIs with rotation-anomaly [21], and so on.

Other than topological insulating phases, various topological semimetals (TSMs) were proposed such as: Dirac semimetals [22–24], Weyl semimetals [25–27], nodal line/loop semimetals [28–30], nodal surface semimetals [31–33], nodal-link semimetals [34–38], and so on. The crystallographic symmetries are also very important as in TCIs while different from TIs/TCIs, the nontrivial band closings occur in the bulk Brillouin zone (BZ) for TSMs. No matter for TCIs or TSMs, the band touching (BT) or band node in the boundary or bulk BZ can result in fascinating consequences such as chiral anomaly [39] and Klein tunneling [40]. Hence, an exhaustive classification of BTs based on group theory is of great importance. To our best knowledge, the exhaustive studies of BTs based on 230 SGs were mainly focused on nodal points [22,41–45], most of which were on nodal points pinned at high-symmetry points (HSPs). Furthermore, compared with nodal point semimetals, the experimental realizations of nodal line/loop/surface semimetals are relatively scarce [46–48] though there have been many first-principles predictions [49–58]. The reasons are as follows. First, the SG symmetry protecting nodal lines/loops/surfaces should be respected in the boundaries to detect surface states related with bulk nodal line/surface structures; Second, the nodal lines/loops/surfaces tend to own finite bandwidth and coexist with other trivial bands in the same energy window in realistic materials. However, the nodal lines/loops/surfaces could cause interesting consequences such as novel long-range Coulomb interaction [59] and intriguing magnetotransport properties [60]. Besides, the surface states of nodal line/loop/surface semimetals are expected to be relatively flat so that electronic interaction could induce instabilities towards superconductivity [61].

Hence, developing a useful guide to find and design nodal line/loop/surface semimetals could benefit realizations of ideal nodal line/loop/surface semimetals that are suitable

*fengtang@nju.edu.cn

for experiments as well as providing a platform with coexisting nontrivial band topology and prominent electron correlation. At the same time, the nodal line/loop or surface TSMs could also serve as a good starting point for creating nodal point TSMs or TIs/TCIs by introducing nontrivial energy gap through spin-orbit coupling (SOC) [26,27] or appropriate external control such as strain and electric and magnetic fields. Very recently, based on crystallographic symmetries, thousands of topological materials by large-scale database searches [62–67] were predicted by symmetry indicators [68,69] or topological quantum chemistry [70]. In the three topological materials databases built in Refs. [62–64], the concrete types of BTs in the category of TSMs are still not clarified clearly, especially for nodal lines/loops/surfaces. To identify a nodal line/loop or surface in a realistic material, conventionally one may firstly clarify the mechanism of forming nodal lines/loops/surfaces and then calculate the corresponding topological invariants such as Chern number or Berry phase [1–6]. Besides, $k \cdot p$ low energy effective models (allowed by symmetries) were usually built to verify the existence of nodal line/loop/surface [1–6]. Obviously, the former method is not very efficient for a large-scale study while the $k \cdot p$ effective models may capture band node of topological origin other than symmetry-enforced one. However, related with the SG symmetries, the breaking of compatibility relations (CRs) can serve as the mechanism or an indicator of BTs in HSPs, high-symmetry lines or planes (HSLs or HSPLs), which is very convenient and the little group of the BT may impose symmetry constraints on the topological character captured from explicit $k \cdot p$ effective model.

In this work, we list all possible SGs with concrete positions hosting nodal lines/loops/surfaces based on the irreducible representations (irreps) of little group of HSLs and HSPLs, and their CRs (hence these nodal lines/loops/surfaces are symmetry-enforced). We focus on four settings as (TRS,SOC) where both TRS and SOC are considered, (TRS,NSOC) where TRS is considered while SOC is neglected, (NTRS,SOC) where TRS is not present while SOC is considered and (NTRS,NSOC) where both TRS and SOC are absent. We also show that from the knowledge of band crossings in the HSL, one can diagnose a nodal loop in a neighboring HSPL or even the configuration of several nodal loops. Similarly, the irrep at HSP can imply a nodal line or surface coinciding with the neighboring HSL or HSPL, respectively. The nodal points lying in HSLs or pinned at HSPs are also found concomitantly. Hence, our work gives a full classification of symmetry-enforced all types of band nodes in 230 SGs. Based on the results of nodal loops implied by the band crossings in HSLs, we propose a practical strategy of realizing Hopf-link semimetal with two nesting nodal loops from an hourglass band structure. The essential cases are highlighted since they are guaranteed to exist by the SG symmetry in corresponding setting in the same spirit of filling-enforced band crossings [71–73].

This paper is organized as follows. In Sec. II, we give a brief overview of CRs in energy bands and sketch the strategy of finding symmetry-enforced nodal points/lines/loops/surfaces using CRs. The main results are also summarized. In Sec. III, we discuss single-valued and double-valued irreps for HSPLs considering the effect of TRS or not, where all possible positions of nodal loops are found which lies in the HSPLs. The HSPLs with degenerate irrep which splits in general direction are nodal surfaces and are further shown to be essential. Then in Sec. IV, we show that many HSLs themselves are (straight) nodal lines. Besides, the band crossing in an HSL may indicate a nodal loop in neighboring HSPL and configurations of several nodal loops in the neighboring HSPLs are discussed. Then Sec. V deals with the irreps at HSPs. Section VI is devoted to the essential results mainly related with the hourglass band connectivity. We then take SGs 34 and 62 as SG examples to demonstrate how to apply our results to figure out all possible nodal lines/loops and highlight two kinds of Hopf-link nodal structures in Secs. VII A and VII B, respectively. The materials realizations of these two kinds of Hopf-link nodal structures are predicted by first-principles calculations in Sec. VII C. Finally Sec. VIII contains conclusions and perspectives.

II. THE STRATEGY AND BRIEF SUMMARY OF THE RESULTS

In this section, we first present a short overview of the CRs for energy bands. Let us assume two associated momenta named by k_1 and k_2 in the BZ, respectively. With no loss of generality, assume that k_1 has an equal or higher symmetry than k_2: for example, $k_1 = (0, 0, 0)$ and $k_2 = (0, 0, k_z)$ so that $k_2 \to k_1$ if $k_z \to 0$. Hence, energy bands originated from one degenerate energy level at k_1 may split in k_2 and the corresponding splitting pattern can be found based on the CRs [74,75]. Such degenerate energy level at k_1 corresponds to some irreps of little group of k_1 [$G(k_1)$], denoted by $D^i_{k_1}$. $D^i_{k_1}$ can be written in the form of a direct sum of the irreps of little group of k_2, $G(k_2)$ with the irreps denoted by $D^j_{k_2}$ as follows:

$$D^i_{k_1} \to \bigoplus_{j=1}^{N_{k_2}} d_j D^j_{k_2}, \tag{1}$$

where N_{k_2} is the total number of different irreps at k_2 and d_j in Eq. (1) is the number of occurrences of $D^j_{k_2}$ in the decomposition which must be non-negative integers. Note that conventional symmetry analysis using operator algebra for representation of an SG is equivalent with the abstract group method [74]. All irreps (single-valued or double-valued) and their CRs of 230 SGs have been listed exhaustively on the Bilbao sever [75,76], based on which we could make an exhaustive study on nodal points/lines/loops/surfaces for all 230 SGs. For nodal points which can be diagnosed by CRs, it is required that away from the BT (which may be located at HSP, or lying in an HSL), the band should split in any direction. On the other hand, once in some direction away from a BT, the band don't split, higher dimensional BT (nodal lines/loops/surfaces) could occur in this direction. Our strategy for identifying the all kinds of BTs is summarized below.

Case (a). k is an HSP. If there exists a degenerate irrep of $G(k)$ and this irrep can decompose into more than one irrep as Eq. (1) in all neighboring HSLs, HSPLs and in general points (GPs), k can thus be a nodal point. Furthermore, If all the irreps of $G(k)$ satisfy the condition, the HSP is thus an essential nodal point. These results are listed in Sec. I A of Ref. [77]. When the point of the HSP contains no achiral

TABLE I. The sections in Ref. [77] for the three types of band nodes.

nodal point	nodal line	nodal loop	nodal surface
Secs. I A, II C	Secs. II A, I B	Secs. III B, II D	Secs. III A, I C, II B

operations, the nodal point [44,78] would be a chiral point. Besides, the degeneracy of the nodal points (as well as other types of band nodes) can be easily obtained and thus given explicitly in our results;

For the rest degenerate irreps, namely, they would not split in some HSLs or HSPLs containing the HSP, which just imply a nodal line (if the irreps split in neighboring HSPLs and GPs) or surface (if the irreps split in GPs) coinciding with the HSL or HSPL, respectively. We list these results in Secs. I B and I C of the SM [77], respectively.

Case (b). k is an HSL. If there exists a degenerate irrep of $G(k)$ and this irrep can decompose into more than one irrep as Eq. (1) in all neighboring HSPLs and in GPs, k can thus be a nodal line (in this work, when we mention "nodal line," the nodal line is straight coinciding with an HSL). Furthermore, if all the irreps of $G(k)$ satisfy the condition, this HSL must be straight nodal line, which means that it is essential. These results are listed in Sec. II A of Ref. [77].

For the rest degenerate irreps, namely, they would not split in some HSPL containing the HSL, which just imply a nodal surface coinciding with the HSPL if the irreps split in GPs. We list these results in Sec. II B of Ref. [77].

Furthermore, when there exist at least two different irreps in the HSL, there could exist a band crossing comprised of these two irreps. For this case, the band crossing could be just a nodal point if the two different irreps are found not to keep being two different irreps in all the neighboring HSPLs. In this case, the nodal point can be a chiral point when the point group of the HSL contains no achiral operations. The results are listed in Sec. II C of Ref. [77]. Otherwise, the band crossing would lie in a nodal loop in the neighboring HSPL, with the results listed in Sec. II D of Ref. [77].

Case (c). k is an HSPL. The same as cases (a) and (b), we should check whether it can own a degenerate irrep which splits into GPs, and if so, k can be a nodal surface. Such nodal surface just coincides with the HSPL. These results are listed in Sec. III A of Ref. [77].

Besides, if there exist two different irreps of $G(k)$, k can thus host a nodal loop of which the Bloch states in the HSPL correspond to these two different irreps of $G(k)$. We list the corresponding results in Sec. III B of Ref. [77].

In Table I, we show the concrete sections where the results for specific type of band node are listed in Ref. [77]. As applications, we propose two Hopf-link structures from our results: one is formed by a straight nodal line threading a nodal loop while the other is formed by two nesting nodal loops. For the former case, all possible results are given in Sec. IV of Ref. [77], from which, we list essential cases in Table II in the main text. For the latter, we first list all possible combinations of two different irreps in HSL in Sec. V of Ref. [77], for which, two bands in the HSL with two different irreps cross each other and the band crossing point could lie in the nodal loop(s) within neighboring HSPL(s) (there are two inequivalent HSPLs containing the HSL). Then if two or more HSPLs containing the HSL could host nodal loops originated from one band crossing in the HSL, these nodal loops would link each other by the band crossing point. On the contrary, if the two nodal loops in the two inequivalent HSPLs are not linked by a point, they have a chance to form a nesting Hopf-link structure as shown in Fig. 1(c3). For this, the band crossing in the HSL could indicate only one nodal loop in one HSPL while there also exists another band crossing in this HSL indicating another nodal loop in another HSPL. These results are listed in Sec. VI of Ref. [77]. Though such situation may not imply a Hopf-link to exist necessarily, we propose a strategy by which we can tune a Hopf-link to appear easily: We can require one nodal loop in the Hopf-link to be essential, for example, due to hourglass band connectivity while the other nodal loop is accidental, as demonstrated in Fig. 1(c3) by a "twisted-hourglass." We list all possible such "twisted hourglasses" in Table III of the main text and also show concrete material example following the strategy.

In the following sections, we first illustrate the irreps in HSPL for which the situation is very simple and the results for nodal surfaces and loops can be obtained.

III. HSPL: BEING NODAL SURFACE OR HOSTING NODAL LOOP

By definition, the little group of the HSPL must contain two elements: identity E and mirror (or glide) M. In general $M^2 = T_{\mathbf{R}}E$ where $T_{\mathbf{R}}$ is a translation operator and the translation $\mathbf{R}$ is the translation part of M^2, parallel with the HSPL. Concretely, for $\mathbf{k}$ in the HSPL, $M^2 \to e^{-i\mathbf{k}\cdot\mathbf{R}}$ so that the eigenvalue of M can be $\lambda_M = \pm e^{-i\mathbf{k}\cdot\mathbf{R}/2}$ or $\lambda_M = \pm ie^{-i\mathbf{k}\cdot\mathbf{R}/2}$, for single and double valued representations, respectively (in other words, for negligible and significant SOC, respectively). In fact, the little group $G(\mathbf{k})$ owns two different irreps corresponding to two opposite eigenvalues of M. Since in the HSPL, the Bloch Hamiltonian $H_{\mathbf{k}}$ commutes with M, each band in the HSPL can be labeled by λ_M or equivalently the irrep of $G(\mathbf{k})$. Note that we don't consider TRS in the above discussion and in this setting, HSPL thus could host a nodal loop when two bands with inverse values of λ_M cross each other. These results are listed for all 230 SGs in Sec. III B of Ref. [77], from which we note that the results for negligible and significant SOC are the same which can be easily understood from above.

Furthermore, since both of the two irreps in the HSPL without TRS are nondegenerate, the HSPL cannot become a nodal surface. However, when considering TRS, one should check whether there exists an SG operator, denoted by β, whose point part being p_β, acts on $\mathbf{k}$ resulting in that $p_\beta\mathbf{k} = -\mathbf{k} + \mathbf{G}$, where $\mathbf{G}$ is an arbitrary reciprocal lattice vector. If this is true, one should check the effect of $T\beta$ (T is the time-reversal operator) on the two irreps of $G(k)$. Then one

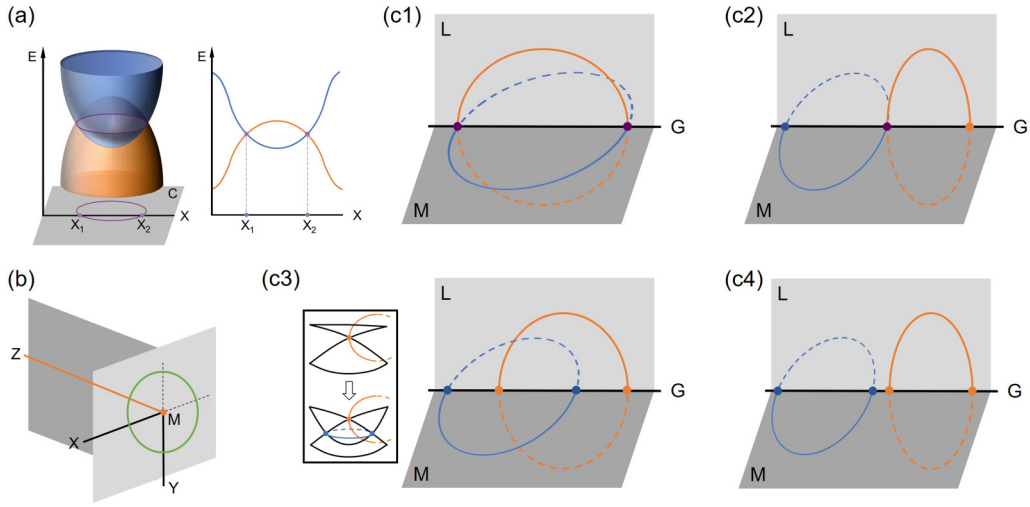

FIG. 1. (a) Demonstration of diagnosing nodal loop from band structure along an HSL. Two bands plotted in different colors in HSPL C cross each other to form a nodal loop indicated by the purple curve. Only from the HSL X $\in$ C, the band structure shown in the right panel clearly shows the band crossing by X_1 and X_2, we can know the existence of a nodal loop lying in C, required by the CRs. (b) The Hopf-link nodal structure consisting of a straight nodal line (itself being an HSL, and here it's MZ) in orange threading a nodal loop (in green) lying in an HSPL (here, MXY) where M is the intersection point of the HSL and HSPL. (c1-c4) Consider two HSPLs, named, by L and M and the intersection of them, the HSL G. L and M could host a nodal loop, respectively. The nodal loops can be diagnosed from the band crossing points lying in G. Owing to the CRs, the symmetry-content of the band crossing, uniquely determine where the resulting nodal loop(s). For (c1), all of the band crossings in G lie in two nodal loops within L and M. For (c2), some band crossing in G can lie in two nodal loops in L and M while some can only lie in one nodal loop within L or M. These two cases correspond to nodal chain structure. For (c3) and (c4), all the band crossings in G can only lie in one nodal loop in L or M, providing the possibility of realizing a nesting Hopf-link nodal structure. In the inset of (c3), we display a twisted hourglass where the top is dragged downward to cross the two necks, resulting in two band crossings (in blue) and form a nodal loop. The nodal loop possibly nests with another one formed by the essential nodal point (in orange) corresponding to the crossing of the two necks.

could be encountered with three possible situations [74] listed in the following: (1) each of the irreps can be related with itself preserving the nondegeneracy; (2) each of the irreps can be related with itself doubling the degeneracy resulting in a two-dimensional (2D) (co-)irrep; or (3) two different irreps are related with each other leading to a 2D (co-)irrep.

Note that in the strict manner we should use "co-irrep" when antiunitary symmetry is considered but we still use the term "irrep" without any ambiguity in this work. The above three situations have been attributed to any irrep of little group on the Bilbao server [75] by the "reality" of the irrep. In the above first two situations, there are still two different irreps in the HSPL while in the third, there is only one irrep. As discussed in case (c) in Sec. II, when two different irreps exist, namely, in the first or second situation, twofold or fourfold degenerate BTs may occur in the HSPL, respectively. Such BTs contain the two different irreps of the HSPL and constitute a nodal loop. On the other hand, when 2D irrep(s) are formed for the second and third situations, the HSPL may become a flat nodal surface if the SG is not centrosymmetric when SOC is included, otherwise the bands in the HSPL would not split in any direction away from the HSPL due to Kramers degeneracy. And when SOC is negligible, all cases in the second and third situations are flat nodal surfaces. The results for all nodal surfaces can be found in Sec. III A of Ref. [77], and it is easy to conclude that they also essentially form nodal surfaces.

IV. HSL: BEING STRAIGHT NODAL LINE OR HOSTING BAND CROSSING LYING IN NODAL LOOP OR IMPLYING A NODAL SURFACE

In the following, we discuss nodal lines/loops which are related with the irreps and CRs in the HSL. Different from HSLs, the point group of HSL may contain c_n rotation with the rotation axis along the HSL, thus more irreps would be found. The same as the above discussion, the HSL may itself form a nodal line. For this case, we also require that the HSL should allow at least one degenerate irrep which splits in any direction away from the HSL. For the effect of antiunitary symmetry $T\beta$ when TRS is considered, it may remove the splitting and thus may turn the original straight nodal line to lie in a nodal surface, or it may create a straight nodal line when it pairs two irreps in the HSL together. For any degenerate irrep in the HSL, it may imply a nodal surface if the irrep keeps being the sole irrep in neighboring HSPL while this irrep splits in GPs.

Besides, two bands with different irreps in the HSL may cross each other resulting a band crossing point in the HSL. Such a band crossing point may simply be a nodal point, namely, the bands split in any direction away from it. Otherwise it must lie in a nodal loop within some HSPL which contains the HSL. In order to know which case to occur, we should firstly know all possible (inequivalent) HSPLs containing the HSL (denoted by k) as shown in Fig. 1(c), denoted by

TABLE II. The SGs allowing Hopf-link structure with essential straight nodal line threading one essential nodal loop within an HSPL. The first column lists the corresponding SGs. The second column contains the positions of HSPLs where the essential nodal loops occur. The third column lists HSLs forming essential straight nodal lines. Note that there is no result for the setting of (TRS,NSOC). Our name convention follows exactly that adopted on the Bilbao server [75] and the coordinates can also be found there.

SG	HSPL	HSL	SG	HSPL	HSL
	Time-reversal symmetry broken, neglecting SOC				
52	L	E	60	W	H
	N	D	61	K	A
	V	H		M	D
54	M	D		V	H
	N	D	62	V	H
56	K	C		W	Q
	L	A	130	B	Y
	M	D		F	U
	N	B	135	E	W
57	K	A	138	B	Y
	L	A		F	U
60	K	A	205	A	ZA
	M	D			
	Time-reversal symmetry broken, considering SOC				
48	K	E	61	L	C
	L	SM		N	B
	M	P		W	G
	N	DT	62	K	E
	V	Q		L	C
	W	LD	126	B	T
50	L	A		E	LD
	N	B		F	DT
	V	Q	130	E	LD
	W	Q	132	E	W
52	L	SM	133	E	V
	M	P		F	DT
	W	LD		F	U
56	V	Q	134	B	T
	W	LD		F	DT
59	V	Q	137	E	V
	W	Q	201	A	T
60	L	E		B	DT
	N	DT	222	B	DT
	W	G			
	Time-reversal symmetric, considering SOC				
29	N	D	61	W	G
	M	D		L	C
30	L	C		N	B
	K	C	62	L	C
31	N	D	102	B	Y
	M	D		F	U
33	K	C	104	B	Y
	M	D		F	U
34	K	C	109	A	Y
	N	B	110	A	Y
	L	A	118	B	Y
	M	D		F	U
60	W	G	122	A	Y
	L	E	205	B	Z

TABLE III. All the positions of the Hopf-link structure formed by two perpendicular nodal loops, one of which is essential nodal loop. The first column lists the corresponding SGs. The second column lists HSLs hosting more than one kind of irreps doublet. In the third and fourth column it contains the positions of two HSPLs where the nodal loops occur. The HSPLs hosting essential nodal loops are marked in red.

SG	HSL	HSPL	
	Time-reversal symmetric, considering SOC		
29	G	L	M
29	Q	L	N
31	G	L	M
31	Q	L	N
33	G	L	M
33	H	K	N
62	Q	L	N
	Time-reversal symmetric, neglecting SOC		
33	Q	L	N
52	P	L	W
	Time-reversal symmetry broken, considering SOC		
52	D	L	V
54	A	M	W
54	E	N	W
56	A	M	W
56	B	K	W
56	C	N	V
56	D	L	V
57	H	K	N
57	Q	L	N
59	C	N	V
59	D	L	V
59	E	N	W
59	P	L	W
60	A	M	W
60	H	K	N
61	A	M	W
61	D	L	V
61	H	K	N
62	B	K	W
62	D	L	V
62	H	K	N
62	Q	L	N
130	U	B	E
137	T	E	F
205	ZA	A	B
	Time-reversal symmetry broken, neglecting SOC		
52	P	L	W
57	B	K	W
57	P	L	W
60	E	N	W
60	G	L	M
61	B	K	W
61	C	N	V
61	G	L	M
62	C	N	V
62	E	N	W
205	Z	A	B

K_a, K_b,... Assume that the band crossing in the HSL contains two different irreps as $D(k)^1$ and $D(k)^2$. Then we should subsequently check whether these two irreps can still maintain to be two different irreps in K_j ($j = a, b, \ldots$) according to the CRs, i.e.,

$$D(k)^1 \to D(K_j)^m, D(k)^2 \to D(K_j)^{m'}, \tag{2}$$

where m, m' denote two different irreps in K_j. If the condition in Eq. (2) is satisfied, there must be a nodal loop in K_j. As shown in Fig. 1(a), two bands with different irreps indicated by different colors in HSPL, C, cross each other to form a nodal loop. Conventionally one need to calculate band structures along many paths in the HSPL to identify the existence of a nodal loop. This method is not very convenient especially when the nodal loop is very small in size. However, as discussed above, one can diagnose nodal loop from band crossing in HSL, and such identification of nodal loop is more operable. As in Fig. 1(a), X $\in$ C, is an HSL and could host different irreps, as denoted by X_1 and X_2, thus allowing robust symmetry-enforced band crossing. This band crossing can be found quickly in the band structure along X in Fig. 1(c). Actually the band crossing containing X_1 and X_2 must lie in a nodal loop in HSPL C, from the knowledge of CRs. We list all doublets of irreps in the HSL exhaustively which could form a band crossing in this HSL and preserve to be two different irreps in the neighboring HSPL, namely resulting in a nodal loop in this HSPL, in Sec. II D of Ref. [77]. In total, there are 466, 466, 428, 194 HSPLs, which can host nodal loops in the settings of (NTRS,NSOC),(NTRS,SOC),(TRS,NSOC),(TRS,SOC), respectively. Among these HSPLs, 440, 356, 398, 185 HSPLs could contain at least one HSL of which the band crossing could imply a nodal loop in the HSPL.

Next we should point out that such simple strategy could be used to find various geometrical structures of different nodal loops. Note that when the HSL has symmetry of c_n when $n = 2, 4, 6$, there would be two inequivalent HSPLs associated with one HSL. And for $n = 3, 4, 6$, c_n could relate one HSPL with the other 2, 1, 2 equivalent HSPLs, respectively. For the latter case, when the band crossing in the HSL which indicates a nodal loop exist, there would be naturally a nodal chain structure formed by the other 2, 1, 2 nodal loops, respectively. In the following, we consider the situations where two inequivalent HSPLs exist, within which two nodal loops have a chance to form a Hopf-link structure.

Possible configurations of nodal loops in several HSPLs

Different from isolated nodal points, nodal loops own more kobs to tune the Fermi surface geometry and its topology. The nodal loops can be isolated, which can be tuned to be gapped or contract into nodal points. Interestingly, the nodal loops can also be linked at a point or nested, allowing more fruitful evolutions under external perturbations. We here proposed that, among the two inequivalent HSPLs that contain the HSL, if both of the two HSPLs could host a nodal loop from the band crossings in the HSL, we can obtain possible configurations of these nodal loops simply from CRs. For simplicity, as shown in Figs. 1(c1)–1(c4), we show two HSPLs where there could exist a nodal loop in respective HSPL. Generally, we could classify the band crossing in the HSL into two types; for one type, it lies in both nodal loops in the two HSPLs while for the other type, it only lies in one HSPL. Obviously, the first type requires that the two nodal loops in the two HSPLs link each other at the band crossing point in the HSL as shown in Fig. 1(c1), forming a nodal chain. For the second type, if all possible band crossings in the HSL result in only one nodal loop in the respective HSPL, the nodal loops must not be linked with each other as shown in Figs. 1(c3) and 1(c4): For Fig. 1(c3), the two nodal loops constitute a Hopf-link nodal structure [79]. Note that for Fig. 1(c2), both of the two types of band crossings in the HSL exist, and it shows another possible configurations forming a nodal chain structure.

Note the inset of Fig. 1(c3). There we show a "twisted hourglass" where the top band of the hourglass is sketched to intersect with the two necking bands, and these two band crossings (in blue) are accidental (while the band crossing (in orange) from the two necks is essential due to the hourglass-band connectivity). When these two accidental band crossings form a nodal loop (in blue) in one HSPL (M), this nodal loop would possibly nest with another nodal loop (in orange, which is originated from the hourglass essential band crossing) in another HSPL (L).

V. HSP: NODAL POINTS OR IMPLYING NODAL LINES/SURFACES

Lastly, we consider the HSPs. Note that different from HSL or HSPL, even though two energy bands at the HSP with two different irreps are tuned to be accidentally degenerate, such BT is easy to be gapped even with small perturbations. In order to own a band node related with the HSP, the HSP must own a degenerate irrep. To guarantee the irrep to constitute a nodal point, it is required that the irrep should split in any direction away from the HSP. And since the HSP owns a higher symmetry than any neighborhood, it is natural to think that the irrep should be split naively. However, this is not always true. If the irrep cannot split to the neighboring HSL, the irrep can be used as the indicator of a nodal line (simply being the HSL), when it is further found that the irrep in the HSL splits in all neighboring HSPLs. Besides, when the irrep in the HSP is found to become one irrep in a neighboring HSPL, it then indicates the nodal surface (simply being the HSPL), when the irrep could split in GPs. Note that the discussions above are all based on CRs, not replying on any $k \cdot p$ models [22,41–43,45], thus the type of band nodes diagnosed from the HSP is not dependent on the cutoff of the $k \cdot p$ expansion.

VI. ESSENTIAL CASES

So far we are mainly concerned with the possible positions in the BZ where the nodal points/lines/loops/surfaces could appear. The identification for them may need further calculations of irreps. However, some of them are found to be essential, which means that they must exist as long as the material belongs to the required SGs in suitable setting even without checking the electronic band structures. We have pointed out that the nodal surfaces as listed in Sec. III A of Ref. [77] are all essential and thus we only discuss essential nodal points/lines (loops) in the following. The essential

cases are of important significance since they are promising to help in predicting ideal semimetals which host band nodes nearly around the Fermi level.

For essential nodal point pinned at HSPs or straight nodal line that coincides with an HSL, it is required that all possible irreps in the HSP/HSL should be degenerate and furthermore, they all split in the neighborhood. The results are printed in red as shown in Secs. I A and II A of SM [77]. For essential nodal points/loops lying in HSLs/HSPLs, we restrict our discussions to those guaranteed by hourglass band connectivity. As discussed in Ref. [80], hourglass band structure can occur in R-X-B where X is HSL or HSPL connecting high-symmetry momenta R and B. When X is an HSPL, the hourglass band connectivity leads to nodal loop in the HSPL, and if the hourglass band connectivity is essential, the nodal loop is thus essential. These results have been summarized in Table IV of Ref. [80] for which each point in the nodal loop corresponds to an hourglass structure. Besides, when X is an HSL, essential hourglass band connectivity could guarantee an band crossing in the HSL. Further analysis on splitting patterns based on CRs (see Sec. IV) could also give rise to essential nodal loop in the neighboring HSPL containing the HSL or simply the essential nodal points. These results are printed in red in Secs. II C and II D of Ref. [77].

VII. APPLICATIONS

Hereafter we focus our discussions on the formation of nodal lines and loops. With the vast body of all possible nodal (loops) organized as in Secs. II A and III B of Ref. [77], one could find materials or systems by fixing the SG symmetry. As long as the required SG symmetry is fulfilled, the system thus has a chance to host nodal lines/loops. Furthermore, if the SG could essentially host nodal lines/loops, the nodal structures must exist. Given concrete types of nodal lines/loops and their positions, we can also design target nodal structures. A straight nodal line threads a nodal loop as shown in Fig. 1(b) forming a Hopf-link [81], for which the essential results are shown in Table II where all the nodal lines and loops are essential. For two nodal loops, as described in Sec. IV A, when two band crossings in an HSL result in two nodal loops lying in two inequivalent HSPLs containing the HSL, there is a chance for the two nodal loops to nest with each other [79]. For materials realization, we propose a more feasible strategy: we first require one nodal loop to be essential, for example, formed by an hourglass band connectivity while the other nodal loop is formed by an accidental band crossing in the hourglass structure. This is schematically shown in the inset of Fig. 1(c3) by a "twisted hourglass." All such hourglasses are listed in Table III. From this table, we find that when the TRS is broken, e.g., in magnetic materials, there is still or even a better chance of realizing the Hopf-link nodal structure. This affords a guide of finding spin-polarized topological Hopf-link semimetals promising in spintronics. In the following, we show two SGs: SGs 34 and 62 and analyze all possible symmetry-enforced nodal lines/loops. Interestingly, they could allow the two kinds of Hopf-link nodal structures regarding nesting structures consisting of one line and one loop or two loops.

A. SG 34: Hopf-link structure of nodal line and loop

In this section, we take SG 34 as examples to demonstrate detailed analysis on all possible nodal lines/loops considering TRS and SOC. In the following, we show in detail how to obtain these results.

SG 34 is nonsymmorphic with two glide planes and the point group of SG 34 is C_{2v} [74], so SG 34 is noncentrosymmetric. The BZ for SG 34 is shown in Fig. 2(a). As listed on the Bilbao server [75], SG 34 owns 12 HSLs as

$$G(1/2,0,w), H(0,1/2,w), LD(0,0,w), Q(1/2,1/2,w), A(u,0,1/2), B(0,v,1/2),$$
$$C(u,1/2,0), D(1/2,v,0), DT(0,v,0), E(u,1/2,1/2), P(1/2,v,1/2), SM(u,0,0),$$

and the following parentheses contain the coordinates adopting the convention in the Bilbao server [75]. Through checking their irreps, we find that LD, Q, A, B, C, D own only one 2D irrep, G and H own four 1D irreps while the rest HSLs own two 1D irreps. For LD, Q, A, B, C, and D, all of them are essential nodal lines since their sole irreps split in neighboring HSPLs. Take the HSL C as the example, the 2D irrep is represented by C3,4 (which means that irreps C3 and C4 are paired considering TRS). HSPLs N (u,1/2,w) and V(u,v,0) can be associated with C, while the irreps of N and V are represented by N3, N4, and V2, respectively, all of which are 1D [75]. Through the CRs [75]:

$$\begin{aligned} &C3,4 \rightarrow N3 + N4, \\ &C3,4 \rightarrow 2V2, \end{aligned} \tag{3}$$

we know that the bands in C must split in N and V, thus C is an essential straight nodal line. The essential nodal lines in HSLs LD, Q, A, B, and D could also be obtained based on similar analysis. The configuration of these nodal lines are displayed in Fig. 2(a) by thick purple lines including S-R (Q), S-X (D), S-Y (C), Z-U (A), Z-GM (LD), and Z-T (B).

Next, let's consider the HSPLs of SG 34, namely, K(0,v,w), L(1/2,v,w), M(u,0,w), N (u,1/2,w), V(u,v,0), and W(u,v,1/2). All of these HSPLs could only host 1D irreps, and K, L, M, N could host two 1D irreps while V and W could only host one. Hence, all these HSPLs cannot be a nodal surface but for K, L, M, N, they could host nodal loops. Furthermore, all these nodal loops are essential and hourglass nodal loops [80]. Here we should point out that they can be related with essential band crossings in related HSLs. For example, the band crossings from irreps DT3 and DT4 in HSL DT must lie in the nodal loops in K, due to

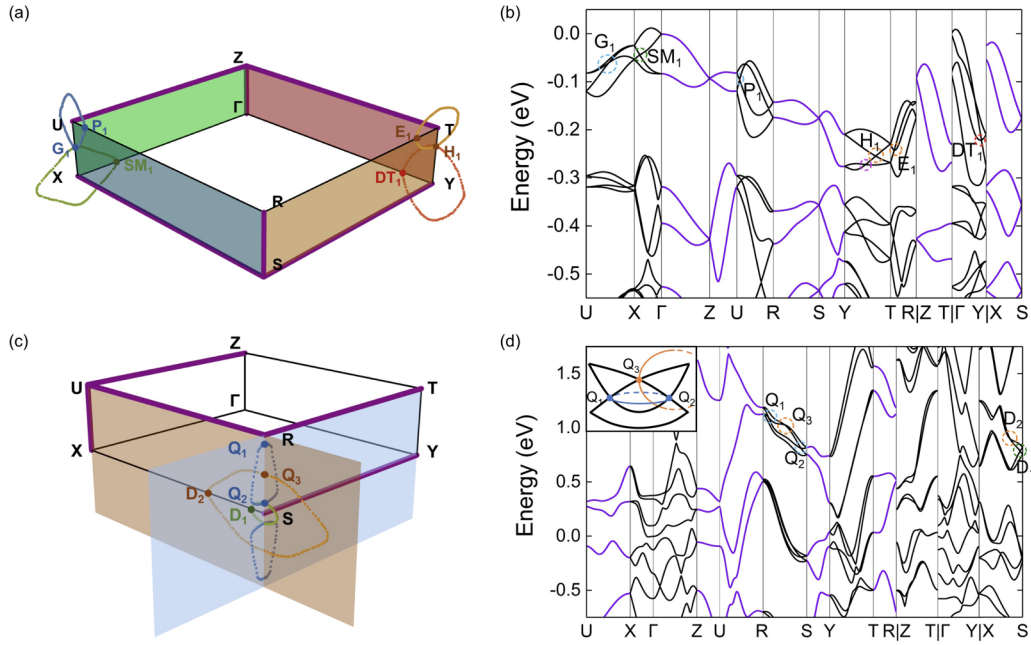

FIG. 2. (a) The BZ of SG 34 (primitive orthorhombic lattice). All possible nodal lines (in purple) are shown as Γ-Z, U-Z, T-Z, S-R, S-Y, and S-X. The band crossing in T-Y (denoted by H_1) lie in two nodal loops in the HSPLs ZY and ST, respectively. Besides, these nodal loops can also be diagnosed from the band crossings E_1 and DT_1, within HSLs T-R and Γ-Y. Here we also demonstrate that the nodal loop around T is threaded by the nodal line Z-T while the nodal loop around Y is threaded by the nodal line S-Y. Similarly, the band crossing in the HSL U-X, denoted by G_1, lie in two nodal loops within two HSPLs, ZX and XR, respectively. These two nodal loops can also be diagnosed by the band crossings of P_1 and SM_1, and they are also threaded by two nodal lines. (b) The first-principles calculated electronic band structure of $B_5Pb_2IO_9$ in SG 34: All related HSLs for nodal lines/loops are chosen. Note that there is an accidental band crossing in HSL Y-T labeled by dashed purple circle, which is further found to be a nodal point. The band structures in the nodal lines are plotted in purple. (c) The BZ of SG 62 (the primitive orthorhombic lattice). The nodal lines are printed in purple including U-Z, U-X, U-R, T-R, and S-Y. Here we show a complex nodal structure comprised of both types of Hopf-links and a nodal chain. The band crossings Q_3 and D_1 are essential which imply two nodal loops within the HSPL RX. The accidental band crossings Q_1 and Q_2 imply a nodal loop in HSPL TS which is linked with the nodal loop from D_1 and nested with the nodal loop from Q_3. Note that the accidental band crossing D_2 also implies the nodal loop from Q_3. (d) The first-principles calculated electronic band structure of $SrAl_2Au_3$ in SG 62 where the band crossings shown in (c) are denoted. The inset shows a twisted hourglass in the HSL R-S. The band structures in the nodal lines are plotted in purple.

that

$$\begin{aligned} &\text{DT3} \rightarrow \text{K3}, \\ &\text{DT4} \rightarrow \text{K4}. \end{aligned} \tag{4}$$

As displayed in Fig. 2(a), four nodal loops lie in HSPLs XZ (M), XR (L), YZ (K), and YR (N). From Sec. II D1 in Ref. [77], we find that, the band crossing in HSL GM-X (SM) indicates an essential nodal loop in the HSPL XZ (M), the band crossings in HSL U-R (P) indicates an essential nodal loop in HSPL XR (L). Note that these band crossings can only indicate one nodal loop. For example, though the HSL U-R (P) lies in HSPL ZR (W), the two irreps in P both decompose to the sole irrep in W, so it is impossible for a robust nodal loop to exist in the HSPL W. Similarly, the band crossing in HSL R-T (E) indicates an essential nodal loop in the HSPL YR (N), the band crossings in HSL GM-Y (DT) indicates an essential nodal loop in HSPL YZ (K) and these band crossings can only indicate one nodal loop. Interestingly, the essential band crossings in HSL U-X (G) originated by G2 + G4 or G3 + G5, both could indicate two essential nodal loops as in Fig. 2(a). Similarly, the essential band crossings in HSL T-Y (H) originated by H2 + H4 or H3 + H5, both could indicate two essential nodal loops as in Fig. 2(a). Hence, the essential band crossings in G or H could indicate a nodal chain structure. Here we highlight the Hopf-link structure when including the essential straight nodal lines in S-X, Z-U, S-Y, and Z-T which just threading the four essential nodal loops shown in Fig. 2(a).

It is worth mentioning that other than the above essential nodal lines/loops, the accidental band crossings in G formed by G2 + G3 or G4 + G5 could only indicate a nodal loop in M while the band crossings formed by G2 + G5 or G3 + G4 could only indicate a nodal loop in L. Similarly, the accidental band crossings in H formed by H2 + H3 or H4 + H5 could only indicate a nodal loop in N while the band crossings formed by H2 + H5 or H3 + H4 could only indicate a nodal loop in K.

B. SG 62: Hopf-link structure of two nodal loops

In the following, we will demonstrate that SG 62 protects the existence of another type of Hopf-link nodal loops. The analyses are as follows. Since SG 62 is centrosymmetric, no symmetry-enforced nodal surface could exist. With respect to nodal lines coinciding with HSLs, we should consider the

HSLs for SG 62, which are the same as those for SG 34. And HSLs A, C, E, G, and P could host only one 4D irrep due to nonsymmorphic symmetries, B, D, and H could host 2 2D irreps, DT, LD, and SM could host only one 2D irrep while Q could host 4 2D irreps. Thus only A, C, E, G, and P could be straight nodal lines since the 2D irreps in other HSLs cannot split in general point due to Kramers degeneracy. They are actually essential straight nodal lines from the CRs on the Bilbao server [75] and displayed in Fig. 2(c) by thick purple lines where A is Z-U, C is S-Y, E is T-R, G is X-U, and P is U-R.

Then investigate the HSPLs. Only HSPLs L (XR), N (YR), and W (ZR) could host nodal loops for they can host two 2D irreps. They are all located in the BZ boundaries. First consider W, and the band crossing formed by the two irreps in HSL Z-T (B) could indicate the nodal loop in W, but the band crossing is not essential. For the rest two HSPLs, namely, L and N, the nodal loop in L is essential while the nodal loop in N is accidental. However, these two nodal loops could form a Hopf-link nodal loop structure as shown in Fig. 2(c). Consider two HSLs, S-X (D) and S-R (Q) that related with L or N and could own band crossings. The two 2D irreps in D must form a band crossing due to the hourglass band connectivity [80] and lie in the nodal loop in the HSPL L as shown by the orange ring in Fig. 2(c). As a matter of fact, such orange ring can also be indicated essentially by the band crossing in the HSL Q, which have four different 2D irreps Q2,2, Q3,3, Q4,4, and Q5,5. In fact, the band crossing by $\mathrm{Q}2, 2+\mathrm{Q}5, 5$ or $\mathrm{Q}3, 3+\mathrm{Q}4, 4$ are essential due to hourglass connectivity [80]. From the CRs as follows:

$$\begin{aligned} &\mathrm{Q}2, 2 \rightarrow \mathrm{L}3, 3, \quad \mathrm{Q}3, 3 \rightarrow \mathrm{L}3, 3, \\ &\mathrm{Q}4, 4 \rightarrow \mathrm{L}4, 4, \quad \mathrm{Q}5, 5 \rightarrow \mathrm{L}4, 4, \\ &\mathrm{Q}2, 2 \rightarrow \mathrm{N}4, 4, \quad \mathrm{Q}3, 3 \rightarrow \mathrm{N}3, 3, \\ &\mathrm{Q}4, 4 \rightarrow \mathrm{N}3, 3, \quad \mathrm{Q}5, 5 \rightarrow \mathrm{N}4, 4, \end{aligned} \tag{5}$$

we know that there is an essential nodal loop within the HSPL L due to band crossing in Q due to $\mathrm{Q}2, 2+\mathrm{Q}5, 5$ or $\mathrm{Q}3, 3+\mathrm{Q}4, 4$. However, such band crossing cannot result in nodal loop in another HSPL N since both Q2,2 and Q5,5 (Q3,3 and Q4,4) decompose to the same irrep N4,4 (N3,3) in N. If the accidental band crossings formed by $\mathrm{Q}2, 2+\mathrm{Q}3, 3$ or $\mathrm{Q}4, 4+\mathrm{Q}5, 5$ as in a "twisted hourglass," the band crossing formed by $\mathrm{Q}2, 2+\mathrm{Q}3, 3$ or $\mathrm{Q}4, 4+\mathrm{Q}5, 5$ can result in only one nodal loop that lies in the HSPL N from Eq. (5). Hence, it is thus possible to realize a Hopf-link structure with the two loops in L and N. Moreover, the nodal loop in the HSPL L is essential which means the nodal loop in L must exist and we only need to tune material parameters (keeping SG symmetry) to make required accidental band crossing in Q, which leads to the other nodal loop in N. It is worth mentioning that for the band crossing by $\mathrm{Q}2, 2+\mathrm{Q}4, 4$ or $\mathrm{Q}3, 3+\mathrm{Q}5, 5$ which is nonessential, it could indicate two nodal loops in the two HSLs L and N, respectively, and result in a nodal chain structure.

C. Nodal line/loop materials

Based on the essential results shown in Secs. II A and III B of Ref. [77] and the Inorganic Crystal Structure Database [82], we find hundreds of promising materials with nodal lines/loops shown in Sec. VII of Ref. [77] (see, also, Refs. [83–88] therein) combined with first-principles calculations, where the concrete positions of the nodal lines/loops near the Fermi level are also given. These materials are all nonmagnetic materials, and their number of elements is less than five. More than half of the materials are binary or ternary compounds. Besides, these materials have relatively band nodes near the Fermi level. It is worth pointing out that Refs. [62–64] diagnosed topological semimetal phase by checking breaking of CRs, not caring too much on the concrete types and positions of the nontrivial band crossings, while here we also check the electronic band structures through detailed band plots and then identify detailed information (shape, energetics etc.) of the nodal lines/loops around the Fermi level. In Sec. IX of Ref. [77], we choose five materials to show the concrete electronic band structures and the nodal loops.

In the following, we take $B_5Pb_2IO_9$ [89] crystallizing in SG 34 and $SrAl_2Au_3$ [90] crystallizing in SG 62 as two materials examples in the main text. These two SGs could showcase various essential nodal loops in several HSPLs with coexisting essential straight nodal lines. Here we highlight that they could present two kinds of Hopf-link structures as discussed above.

Firstly we showcase $B_5Pb_2IO_9$ [89] crystallizing in SG 34 with orthorhombic lattice, whose first-principles calculated band structure is shown in Fig. 2(b), where the k-paths are chosen to cover the theoretical predicted k·*s* which could be essential nodal line or host essential band crossing implying a nodal loop, as in Sec. VII A. From the band structure in HSLs U-X (G), U-R (P), Γ-X (SM), T-Y (H), T-R (E), and Γ-Y (DT), we can find essential hourglass band crossings label as G_1, P_1, SM_1, H_1, E_1 and DT_1 respectively. As shown in the above, these band crossings could imply nodal loops in respective HSPLs: G_1 and H_1 indicate two nodal loops in two perpendicular HSPLs (thus forming a nodal chain) while the rest band crossings only lie in one nodal loop within corresponding HSPL. These nodal loops from first-principles calculations are demonstrated in Fig. 2(a) by green or orange cicles. Besides, the nodal lines that coincide with HSLs are plotted in purple in the BZ where the electronic band structure is also shown by purple curves in Fig. 2(b). Other than the nodal chain structures, the straight nodal line threading the nodal loop also constitute a Hopf-link structure.

Next we showcase the materials $SrAl_2Au_3$ [90] crystallizing in SG 62 with orthorhombic lattice, whose first-principles calculated electronic band structure and fascinating nodal loop structure are shown in Figs. 2(d) and 2(c), respectively. The band crossings in S-X (D) and S-R (Q) that are relevant with the nodal loops we display are denoted by orange or green dashed circle in Fig. 2(d). These band crossings are also named by D_i, Q_j $(i = 1, 2, j = 1, 2, 3)$ labeled near the dashed circles. Based on first-principles results, we find that D_1 and D_2 contain the irreps $\mathrm{D}2, 3+\mathrm{D}4, 5$ while Q_1, Q_2, Q_3 contain irreps of $\mathrm{Q}4, 4+\mathrm{Q}5, 5$, $\mathrm{Q}2, 2+\mathrm{Q}4, 4$, $\mathrm{Q}2, 2+\mathrm{Q}5, 5$, respectively. We also show these nodes in Fig. 2(c) in the BZ, exactly corresponding to those in Fig. 2(d). Consistent with the above theoretical analysis, it can be found that

along with the band nodes of D_i, Q_j $(i = 1, 2, j = 1, 2, 3)$, there exist four nodal loops forming very intriguing structures: The orange nodal loops from D_2 and Q_3 is essential (Q_3 is essential while D_2 is not), which is nested with the $Q_{1,2}$ related nonessential nodal loops. Note that Q_2 also indicates another nodal loop in green so that the blue nodal loops are linked with the green one. Interestingly, the green nodal loop contains a band crossing D_1 which is essential. Since these nodal loops are not very far from the Fermi level, this material is thus expected to be experimentally studied on the predicted nodal loops and the related consequences in future.

VIII. CONCLUSIONS AND PERSPECTIVES

We study exhaustively all types of band nodes based on CRs for all 230 SGs. The single-valued and doubled irreps are considered with respect to spin-orbit coupled and free systems, respectively. And the TRS is also considered to affect the irreps and CRs, which could lead to significant effects on the formation of nodal loops and surfaces in HSPLs. The nodal surfaces we found are all enforced by crystallographic symmetries. For these flat nodal surfaces, TRS should be considered otherwise the HSPL only own two nondegenerate irreps. Besides, the SGs allowing flat nodal surfaces should be noncentrosymmetric when SOC is also included. Also, these nodal surfaces are found to be all essential. Furthermore, the HSPLs which own two different irreps whether TRS is considered or not could host a nodal loop. We also study straight nodal lines coinciding with the HSLs, some of which are found to be essential. The band crossing in an HSL and the irrep at HSP can be exploited to diagnose nodal loops in a convenient way. The essential band crossings in HSLs indicating nodal loops in neighboring HSPLs and these essential nodal loops enforced by hourglass band connectivity are also given. When the band crossing in the HSL cannot imply a nodal loop, it is just a nodal point. The irreps at HSP can not only imply nodal lines/surfaces, they can also be a nodal point. Finally, we take SGs 34 and 62 as the examples to demonstrate comprehensive analysis on all possible nodal lines/loops based on our results in Ref. [77]. Interestingly, these two SGs could host two kinds of Hopf-link nodal structures formed by a nodal line and a nodal loop, or formed by two nodal loops. $B_5Pb_2IO_9$ in SG 34 and $SrAl_2Au_3$ in SG 62 can host these two kinds of novel Hopf-link structures, respectively. The promising SGs for these two kinds of Hopf-link structures are listed in the main text, respectively. These results are expected to be used in designing artificial systems that can own such Hopf-link structure, simply based on the crystal symmetry. They also throw light on constructing low-energy models with Hopf links.

It is worth mentioning that our results can be also used to find materials realizations other than nonmagnetic electronic systems. Besides, type-III and IV magnetic SGs are out of our scope of study, but our strategy can be easily generalized to these settings once their CRs are obtained. And 80 layer groups for 2D materials or surfaces of 3D materials, though being the subsets of 230 SGs, could bring about nontrivial results since the high-symmetry momenta for layer groups are much simpler than SG cases thus the HSPLs accommodating the nodal loops in SGs may not exist in layer groups. We expect that our tables for all types of symmetry-enforced band nodes can be applied to the design for more new and even ideal semimetals with targeted nodal structure in near future.

Note added. Recently, Ref. [91] appeared, which is based on a similar idea and discusses the superconducting nodes pinned to any line in momentum space. However, this work is different from Ref. [91] in terms of the formulation and the mathematical approach adopted. We give an exhaustive search for all types of band nodes and a scheme of the realization of the Hopf-link structure, which affords a guide of finding specific topological semimetals.

ACKNOWLEDGMENTS

We were supported by the National Key R&D Program of China (Grants No. 2017YFA0303203 and No. 2018YFA0305704), the National Natural Science Foundation of China (NSFC Grants No. 11525417, no. 11834006, No. 51721001, and No. 11790311) and the excellent program at Nanjing University. X.W. also acknowledges the support from the Tencent Foundation through the XPLORER PRIZE. F.T. was supported by the Fundamental Research Fund for the Central Universities (Grants No. 14380144 and No. 14380157) and thanks Dingyu Xing and Baigen Wang for their kind and substantial support on scientific research. F.T. also thanks stimulating discussions with Wei Chen.

[1] X.-L. Qi and S.-C. Zhang, Topological insulators and superconductors, Rev. Mod. Phys. **83**, 1057 (2011).
[2] M. Z. Hasan and C. L. Kane, *Colloquium:* topological insulators, Rev. Mod. Phys. **82**, 3045 (2010).
[3] A. Bansil, H. Lin, and T. Das, *Colloquium:* topological band theory, Rev. Mod. Phys. **88**, 021004 (2016).
[4] N. P. Armitage, E. J. Mele, and A. Vishwanath, Weyl and Dirac semimetals in three-dimensional solids, Rev. Mod. Phys. **90**, 015001 (2018).
[5] Y. Ando, Topological insulator materials, J. Phys. Soc. Jpn. **82**, 102001 (2013).
[6] T. O. Wehling, A. M. Black-Schaffer, and A. V. Balatsky, Dirac materials, Adv. Phys. **63**, 1 (2014).
[7] A. P. Schnyder, S. Ryu, A. Furusaki, and A. W. W. Ludwig, Classification of topological insulators and superconductors in three spatial dimensions, Phys. Rev. B **78**, 195125 (2008).
[8] A. Kitaev, Periodic table for topological insulators and superconductors, AIP Conf. Proc. **1134**, 22 (2009).
[9] L. Fu and C. L. Kane, Topological insulators with inversion symmetry, Phys. Rev. B **76**, 045302 (2007).
[10] C.-K. Chiu, J. C. Y. Teo, A. P. Schnyder, and S. Ryu, Classification of topological quantum matter with symmetries, Rev. Mod. Phys. **88**, 035005 (2016).
[11] J. Kruthoff, J. de Boer, J. van Wezel, C. L. Kane, and R.-J. Slager, Topological Classification of Crystalline Insulators

through Band Structure Combinatorics, Phys. Rev. X **7**, 041069 (2017).
[12] R.-J. Slager, A. Mesaros, V. Juričić, and J. Zaanen, The space group classification of topological band-insulators, Nat. Phys. **9**, 98 (2013).
[13] L. Fu, Topological Crystalline Insulators, Phys. Rev. Lett. **106**, 106802 (2011).
[14] Y. Ando and L. Fu, Topological crystalline insulators and topological superconductors: From concepts to materials, Annu. Rev. Condens. Matter Phys. **6**, 361 (2015).
[15] T. H. Hsieh, H. Lin, J. Liu, W. Duan, A. Bansil, and L. Fu, Topological crystalline insulators in the SnTe material class, Nat. Commun. **3**, 982 (2012).
[16] Z. Wang, A. Alexandradinata, R. J. Cava, and B. Andrei Bernevig, Hourglass fermions, Nature (London) **532**, 189 (2016).
[17] J. Langbehn, Y. Peng, L. Trifunovic, F. von Oppen, and P. W. Brouwer, Reflection Symmetric Second-Order Topological Insulators and Superconductors, Phys. Rev. Lett. **119**, 246401 (2017).
[18] Z. Song, Z. Fang, and C. Fang, $(d-2)$-Dimensional Edge States of Rotation Symmetry Protected Topological States, Phys. Rev. Lett. **119**, 246402 (2017).
[19] F. Schindler, A. M. Cook, M. G. Vergniory, Z. Wang, S. S. P. Parkin, B. A. Bernevig, and T. Neupert, Higher-order topological insulators, Sci. Adv. **4**, eaat0346 (2018).
[20] W. A. Benalcazar, B. A. Bernevig, and T. L. Hughes, Electric multipole moments, topological multipole moment pumping, and chiral hinge states in crystalline insulators, Phys. Rev. B **96**, 245115 (2017).
[21] C. Fang and L. Fu, New classes of topological crystalline insulators having surface rotation anomaly, Sci. Adv. **5**, eaat2374 (2019).
[22] S. M. Young, S. Zaheer, J. C. Y. Teo, C. L. Kane, E. J. Mele, and A. M. Rappe, Dirac Semimetal in Three Dimensions, Phys. Rev. Lett. **108**, 140405 (2012).
[23] Z. Wang, Y. Sun, X.-Q. Chen, C. Franchini, G. Xu, H. Weng, X. Dai, and Z. Fang, Dirac semimetal and topological phase transitions in A_3Bi (A = Na, K, Rb), Phys. Rev. B **85**, 195320 (2012).
[24] Z. Wang, H. Weng, Q. Wu, X. Dai, and Z. Fang, Three-dimensional Dirac semimetal and quantum transport in Cd_3As_2, Phys. Rev. B **88**, 125427 (2013).
[25] X. Wan, A. M. Turner, A. Vishwanath, and S. Y. Savrasov, Topological semimetal and Fermi-arc surface states in the electronic structure of pyrochlore iridates, Phys. Rev. B **83**, 205101 (2011).
[26] H. Weng, C. Fang, Z. Fang, B. A. Bernevig, and X. Dai, Weyl Semimetal Phase in Noncentrosymmetric Transition-Metal Monophosphides, Phys. Rev. X **5**, 011029 (2015).
[27] S.-M. Huang, S.-Y. Xu, I. Belopolski, C.-C. Lee, G. Chang, B. Wang, N. Alidoust, G. Bian, M. Neupane, C. Zhang, S. Jia, A. Bansil, H. Lin, and M. Z. Hasan, A Weyl fermion semimetal with surface Fermi arcs in the transition metal monopnictide TaAs class, Nat. Commun. **6**, 7373 (2015).
[28] A. A. Burkov, M. D. Hook, and L. Balents, Topological nodal semimetals, Phys. Rev. B **84**, 235126 (2011).
[29] C. Fang, Y. Chen, H.-Y. Kee, and L. Fu, Topological nodal line semimetals with and without spin-orbital coupling, Phys. Rev. B **92**, 081201(R) (2015).
[30] T. Bzdušek, Q. Wu, A. Rüegg, M. Sigrist, and A. A. Soluyanov, Nodal-chain metals, Nature (London) **538**, 75 (2016).
[31] Q.-F. Liang, J. Zhou, R. Yu, Z. Wang, and H. Weng, Node-surface and node-line fermions from nonsymmorphic lattice symmetries, Phys. Rev. B **93**, 085427 (2016).
[32] W. Wu, Y. Liu, S. Li, C. Zhong, Z.-M. Yu, X.-L. Sheng, Y. X. Zhao, and S. A. Yang, Nodal surface semimetals: Theory and material realization, Phys. Rev. B **97**, 115125 (2018).
[33] C. Zhong, Yuanping Chen, Y. Xie, S. A. Yang, M. L. Cohenc, and S. B. Zhang, Towards three-dimensional Weyl-surface semimetals in graphene networks, Nanoscale **8**, 7232 (2016).
[34] W. Chen, H.-Z. Lu, and J.-M. Hou, Topological semimetals with a double-helix nodal link, Phys. Rev. B **96**, 041102(R) (2017).
[35] Z. Yan, R. Bi, H. Shen, L. Lu, S.-C. Zhang, and Z. Wang, Nodal-link semimetals, Phys. Rev. B **96**, 041103(R) (2017).
[36] M. Ezawa, Topological semimetals carrying arbitrary Hopf numbers: Fermi surface topologies of a Hopf link, Solomon's knot, trefoil knot, and other linked nodal varieties, Phys. Rev. B **96**, 041202(R) (2017).
[37] P.-Y. Chang and C.-H. Yee, Weyl-link semimetals, Phys. Rev. B **96**, 081114(R) (2017).
[38] Z. Yang, C.-K. Chiu, C. Fang, and J. Hu, Jones Polynomial and Knot Transitions in Hermitian and Non-Hermitian Topological Semimetals, Phys. Rev. Lett. **124**, 186402 (2020).
[39] V. Aji, Adler-Bell-Jackiw anomaly in Weyl semimetals: Application to pyrochlore iridates, Phys. Rev. B **85**, 241101(R) (2012).
[40] M. I. Katsnelson, K. S. Novoselov, and A. K. Geim, Chiral tunnelling and the Klein paradox in graphene, Nat. Phys. **2**, 620 (2006).
[41] J. L. Mañes, Existence of bulk chiral fermions and crystal symmetry, Phys. Rev. B **85**, 155118 (2012).
[42] B. Bradlyn, J. Cano, Z. Wang, M. G. Vergniory, C. Felser, R. J. Cava, and B. A. Bernevig, Beyond Dirac and Weyl fermions: Unconventional quasiparticles in conventional crystals, Science **353**, aaf5037 (2016).
[43] B. J. Wieder, Y. Kim, A. M. Rappe, and C. L. Kane, Double Dirac Semimetals in Three Dimensions, Phys. Rev. Lett. **116**, 186402 (2016).
[44] G. Chang, B. J. Wieder, F. Schindler, D. S. Sanchez, I. Belopolski, S.-M. Huang, B. Singh, D. Wu, T.-R. Chang, T. Neupert, S.-Y. Xu, H. Lin, and M. Z. Hasan, Topological quantum properties of chiral crystals, Nat. Mater. **17**, 978 (2018).
[45] B.-J. Yang and N. Nagaosa, Classification of stable three-dimensional Dirac semimetals with nontrivial topology, Nat. Commun. **5**, 4898 (2014).
[46] G. Bian, T.-R. Chang, R. Sankar, S.-Y. Xu, H. Zheng, T. Neupert, C.-K. Chiu, S.-M. Huang, G. Chang, I. Belopolski, D. S. Sanchez, M. Neupane, N. Alidoust, C. Liu, B. Wang, C.-C. Lee, H.-T. Jeng, C. Zhang, Z. Yuan, S. Jia, A. Bansil, F. Chou, H. Lin, and M. Z. Hasan, Topological node-line fermions in spin-orbit metal $PbTaSe_2$, Nat. Commun. **7**, 10556 (2016).
[47] J. Hu, Z. Tang, J. Liu, X. Liu, Y. Zhu, D. Graf, K. Myhro, S. Tran, C. N. Lau, J. Wei, and Z. Mao, Evidence of Topological Nodal-Line Fermions in ZrSiSe and ZrSiTe, Phys. Rev. Lett. **117**, 016602 (2016).
[48] W. Chen, L. Liu, W. Yang, D. Chen, Z. Liu, Y. Huang, T. Zhang, H. Zhang, Z. Liu, and D. W. Shen, Evidence of topological nodal lines and surface states in the centrosymmetric superconductor $SnTaS_2$, Phys. Rev. B **103**, 035133 (2021).

[49] H. Weng, Y. Liang, Q. Xu, R. Yu, Z. Fang, X. Dai, and Y. Kawazoe, Topological node-line semimetal in three-dimensional graphene networks, Phys. Rev. B **92**, 045108 (2015).

[50] R. Yu, H. Weng, Z. Fang, X. Dai, and X. Hu, Topological Node-Line Semimetal and Dirac Semimetal State in Antiperovskite Cu_3PdN, Phys. Rev. Lett. **115**, 036807 (2015).

[51] Y. Kim, B. J. Wieder, C. L. Kane, and A. M. Rappe, Dirac Line Nodes in Inversion-Symmetric Crystals, Phys. Rev. Lett. **115**, 036806 (2015).

[52] Y. P. Du, F. Tang, D. Wang, L. Sheng, E. J. Kan, C. G. Duan, S. Y. Savrasov, and X. G. Wan, CaTe: A new topological node-line and Dirac semimetal, npj Quantum Mater. **2**, 3 (2017).

[53] S. Li, Y. Liu, S. S. Wang, Z. M. Yu, S. Guan, X. L. Sheng, Y. G. Yao, and S. A. Yang, Nonsymmorphic-symmetry-protected hourglass Dirac loop, nodal line, and Dirac point in bulk and monolayer X_3SiTe_6(X = Ta, Nb), Phys. Rev. B **97**, 045131 (2018).

[54] J.-M. Carter, V. V. Shankar, M. A. Zeb, and H.-Y. Kee, Semimetal and topological insulator in perovskite iridates, Phys. Rev. B **85**, 115105 (2012).

[55] L. M. Schoop, M. N. Ali, C. Straer, A. Topp, A. Varykhalov, D. Marchenko, V. Duppel, S. S. P. Parkin, B. V. Lotsch, and C. R. Ast, Dirac cone protected by non-symmorphic symmetry and three-dimensional Dirac line node in ZrSiS, Nat. Commun **7**, 11696 (2016).

[56] S.-S. Wang, Y. Liu, Z.-M. Yu, X.-L. Sheng, and S. A. Yang, Hourglass Dirac chain metal in rhenium dioxide, Nat. Commun. **8**, 1844 (2017).

[57] D. Shao, H. Wang, T. Chen, P. Lu, Q. Gu, L. Sheng, D. Xing, and J. Sun, Composite topological nodal lines penetrating the Brillouin zone in orthorhombic AgF_2, npj Comput. Mater. **5**, 53 (2019).

[58] D. Shao and C. Fang, Filling-enforced Dirac nodal loops in nonmagnetic systems and their evolutions under various perturbations, Phys. Rev. B **102**, 165135 (2020).

[59] E.-G. M. Yejin Huh and Y. B. Kim, Long-range Coulomb interaction in nodal-ring semimetals, Phys. Rev. B **93**, 035138 (2016).

[60] S. Chen, Z. Lou, Y. Zhou, Q. Chen, B. Xu, C. Wu, J. Du, J. Yang, H. Wang, and M. Fang, Magnetoresistance and Kondo effect in nodal-line semimetal VAs_2, Chin. Phys. Lett. **38**, 017202 (2021).

[61] T. T. Heikkila and G. E. Volovik, Flat bands as a route to high-temperature superconductivity in graphite, in *Basic Physics of Functionalized Graphite*, edited by P. Esquinazi, Springer Series in Materials Science Vol. 244 (Springer, Cham, 2016).

[62] T. Zhang, Y. Jiang, Z. Song, H. Huang, Y. He, Z. Fang, H. Weng, and C. Fang, Catalogue of topological electronic materials, Nature (London) **566**, 475 (2019).

[63] M. G. Vergniory, L. Elcoro, C. Felser, N. Regnault, B. A. Bernevig, and Z. Wang, A complete catalogue of high-quality topological materials, Nature (London) **566**, 480 (2019).

[64] F. Tang, H. C. Po, A. Vishwanath, and X. Wan, Comprehensive search for topological materials using symmetry indicators, Nature (London) **566**, 486 (2019).

[65] F. Tang, H. C. Po, A. Vishwanath, and X. Wan, Topological materials discovery by large-order symmetry indicators, Sci. Adv. **5**, eaau8725 (2019).

[66] D. Wang, F. Tang, J. Ji, W. Zhang, A. Vishwanath, H. C. Po, and X. Wan, Two-dimensional topological materials discovery by symmetry-indicator method, Phys. Rev. B **100**, 195108 (2019).

[67] J. Gao, Y. Qian, S. Nie, Z. Fang, H. Weng, and Z. Wang, High-throughput screening for Weyl semimetals with S_4 symmetry, Sci. Bulletin **66**, 667 (2021).

[68] H. C. Po, A. Vishwanath, and H. Watanabe, Symmetry-based indicators of band topology in the 230 space groups, Nat. Commun. **8**, 50 (2017).

[69] F. Tang, H. C. Po, A. Vishwanath, and X. Wan, Efficient topological materials discovery using symmetry indicators, Nat. Phys. **15**, 470 (2019).

[70] B. Bradlyn, L. Elcoro, J. Cano, M. G. Vergniory, Z. Wang, C. Felser, M. I. Aroyo, and B. A. Bernevig, Topological quantum chemistry, Nature (London) **547**, 298 (2017).

[71] H. Watanabe, H. C. Po, M. P. Zaletel, and A. Vishwanath, Filling-Enforced Gaplessness in Band Structures of the 230 Space Groups, Phys. Rev. Lett. **117**, 096404 (2016).

[72] R. Chen, H. C. Po, J. B. Neaton, and A. Vishwanath, Topological materials discovery using electron filling constraints, Nat. Phys. **14**, 55 (2017).

[73] D. Wang, F. Tang, H. C. Po, A. Vishwanath, and X. Wan, XFe_4Ge_2 (X=Y, Lu) and Mn_3Pt: Filling-enforced magnetic topological metals, Phys. Rev. B **101**, 115122 (2020).

[74] C. J. Bradley and A. P. Cracknell, *The Mathematical Theory of Symmetry in Solids: Representation Theory for Point Groups and Space Groups* (Oxford University Press, Oxford, 1972).

[75] http://www.cryst.ehu.es.

[76] Using the CRs for 230 SGs negletcing the effect of TRS, we can obtain the CRs including TRS based on the pairing or not of irreps of little group by TRS.

[77] See Supplemental Material at http://link.aps.org/supplemental/10.1103/PhysRevB.104.045107, which contains the exhaustive results for all symmetry-enforced nodal points, nodal lines and nodal surfaces for materials with/without TRS and significant/negligible SOC. We also list the realistic materials which could host nodal lines or nodal loops near the Fermi level, and show the band structures for the selected examples.

[78] P. Tang, Q. Zhou, and S.-C. Zhang, Multiple Types of Topological Fermions in Transition Metal Silicides, Phys. Rev. Lett. **119**, 206402 (2017).

[79] G. Chang, S.-Y. Xu, X. Zhou, S.-M. Huang, B. Singh, B. Wang, I. Belopolski, J. Yin, S. Zhang, A. Bansil, H. Lin, and M. Z. Hasan, Topological Hopf and Chain Link Semimetal States and Their Application to Co_2MnGa, Phys. Rev. Lett. **119**, 156401 (2017).

[80] L. Wu, F. Tang, and X. Wan, Exhaustive list of topological hourglass band crossings in 230 space groups, Phys. Rev. B **102**, 035106 (2020).

[81] G. E. Volovik and K. Zhang, Lifshitz transitions, type-II Dirac and Weyl fermions, event horizon and all that, J. Low Temp. Phys. **189**, 276 (2017).

[82] M. Hellenbrandt, The Inorganic Crystal Structure Database (ICSD)—Present and future, Crystallogr. Rev. **10**, 17 (2004).

[83] P. Blaha, K. Schwarz, G. K. H. Madsen, D. Kvasnicka, and J. Luitz, *Wien2k, An Augmented Plane Wave + Local Orbitals Program for Calculating Crystal Properties* (Karlheinz Schwarz, Technische Univ. Wien, Austria, 2001).

[84] J. L. Roy, J.-M. Moreau, D. Paccard, and E. Parthé, Rare-earth (and yttrium)-iridium and -platinum compounds with the Fe_3C structure type, Acta Cryst. B **35**, 1437 (1979).

[85] R. Arpe and H. Muller-Buschbaum, About Bi_2PdO_4, Z. Naturforsch. **31b**, 1708 (1976).

[86] V. R. Arpe and H. Müller-Buschbaum, Isolierte quadratisch planare $(CuO_4)^{6-}$-polyeder in $CuBi_2O_4$, ein neuer bautyp zur formel $(Me^{3+})_2M^{2+}O_4$, Z. Anorg. Allg. Chem. **426**, 1 (1976).

[87] M. F. Zumdick and R. Pöttgen, Determination of the superstructures for the stannides ZrIrSn, HfCoSn, and HfRhSn, Z. Kristallogr. **214**, 90 (1999).

[88] S. Jobic, R. Brec, A. Pasturel, H.-J. Koo, and M.-H. Whangbo, Theoretical study of possible iridium ditelluride phases attainable under high pressure, J. Solid State Chem. **162**, 63 (2001).

[89] Y.-Z. Huang, L.-M. Wu, X.-T. Wu, L.-H. Li, L. Chen, and Y.-F. Zhang, $Pb_2B_5O_9I$: An iodide borate with strong second harmonic generation, J. Am. Chem. Soc. **132**, 12788 (2010).

[90] G. Birgit and P. Rainer, Alkaline earth-gold-aluminides: synthesis and structure of $SrAu_3Al_2$, $SrAu_{2.83}Al_{2.17}$, $BaAu_{2.89}Al_{2.11}$ and $BaAu_{7.09}Al_{5.91}$, Z. Kristallogr. **70b**, 903 (2015).

[91] S. Ono and K. Shiozaki, Symmetry-based approach to nodal structures: Unification of compatibility relations and point-node classifications, arXiv:2102.07676.